Received: 17 December 2017 | Revised: 4 July 2018 | Accepted: 28 September 2018

DOI: 10.1002/nla.2220

RESEARCH ARTICLE

WILEY

A parallel time integrator for solving the linearized shallow water equations on the rotating sphere

Martin Schreiber[1,2] | Richard Loft[3]

[1]College of Engineering, Mathematics and Physical Sciences, University of Exeter, Exeter, UK

[2]Chair of Computer Architecture and Parallel Systems, Technical University of Munich, Germany

[3]Computational and Information Systems Laboratory, National Center for Atmospheric Research, Boulder, Colorado

Correspondence
Martin Schreiber, College of Engineering, Mathematics and Physical Sciences, University of Exeter, North Park Road, Harrison Building, Exeter EX4 4QF, UK.
Email: schreiberx@gmail.com

Funding information
National Science Foundation

Summary

With the stagnation of processor core performance, further reductions in the time to solution for geophysical fluid problems are becoming increasingly difficult with standard time integrators. Parallel-in-time exposes and exploits additional parallelism in the time dimension, which is inherently sequential in traditional methods. The rational approximation of exponential integrators (REXI) method allows taking arbitrarily long time steps based on a sum over a number of decoupled complex PDEs that can be solved independently massively parallel. Hence, REXI is assumed to be well suited for modern massively parallel super computers, which are currently trending. To date, the study and development of the REXI approach have been limited to linearized problems on the periodic two-dimensional plane. This work extends the REXI time stepping method to the linear shallow-water equations on the rotating sphere, thus moving the method one step closer to solving fully nonlinear fluid problems of geophysical interest on the sphere. The rotating sphere poses particular challenges for finding an efficient solver due to the zonal dependence of the Coriolis term. Here, we present an efficient REXI solver based on spherical harmonics, showing the results of a geostrophic balance test, a comparison with alternative time stepping methods, an analysis of dispersion relations indicating superior properties of REXI, and finally, a performance comparison on the Cheyenne supercomputer. Our results indicate that REXI not only can take larger time steps but also can be used to gain higher accuracy and significantly reduced time to solution compared with currently existing time stepping methods.

KEYWORDS

high-performance computing, massively parallel, parallel-in-time, rational approximation of exponential integrator, shallow-water equations on the rotating sphere, spherical harmonics

1 | INTRODUCTION

The current trend in computer architectures is toward increasing levels of parallelism while maintaining constant or even reducing individual core performance. These developments, in place now for over a decade, pose new challenges

for the development of faster solvers for nonlinear partial differential equation problems. Such problems are found in the solvers, or dynamical cores, used in modeling the geophysical fluids in the areas of climate, weather, etc. Accelerating such problems in the post–Dennard scaling[1*] era is a grand challenge of the highest societal importance and is the focus of this paper.

Overcoming the time step restrictions of time integration methods while maintaining sufficient accuracy requires more sophisticated time-integration approaches, which generally focus on taking bigger time steps. Parallel-in-time (PinT) methods are one class of such methods (see the work of Gander[2] for an overview). A scalable PinT method called the rational approximation of an exponential integrator (T-REXI[†]) was recently developed and explored for simulations of linear operators on the biperiodic plane.[3,4] In this work, we will investigate the application of T-REXI to the linear shallow-water equations (SWEs) on the rotating sphere. The nonlinear SWEs are an important test case in the development of dynamical cores in the atmospheric sciences; thus, this work brings the T-REXI method significantly closer to modeling of planetary-scale geophysical fluid problems.

1.1 | Related work

An alternative to the T-REXI approach to solving the linear SWE on the rotating sphere is computing the solution for the linear operator directly with an eigenvalue/vector factorization, resulting in a set of independent ODEs (see, e.g., the work of Hochbruck et al.[5]), which can then be trivially solved with a direct time integration of the form $\hat{u}(t) = \exp(\lambda t)\hat{u}(0)$ with $\hat{u}(t)$ being the solution at time t after transformation to eigenvector space and λ being the corresponding eigenvalue. An eigenfactorization based on using spherical harmonics (SH) for the basis leads to the *Hough functions* (see, e.g., the works of Kasahara[6] and Wang et al.[7]), which are eigenfunctions of the SWE on the rotating sphere. However, the matrices of the discretized eigenfunctions are dense and therefore have storage requirements, which are quadratic in the number of degrees of freedom, that is, the total number of SH basis functions kept in the expansion. Running computations with the Hough functions is indeed feasible for very low resolutions but inefficient for high resolution models due to these quadratic storage and related computational requirements.

One of the main focus of the present work is to overcome time step restrictions in atmospheric simulations. Besides the CFL restrictions mentioned earlier, the mathematical properties of the SWEs lead to further restrictions: Specifically, one finds that the gravitation-related parts of the equations are the fastest evolving and, thus, the most restrictive ones, requiring about six times smaller time steps compared to the meteorological modes, for example, modes that are related to Rossby waves (see the work of Robert[8]). Broadly speaking, two different approaches have been identified to overcome the time step restrictions of the SWEs on the rotating sphere. The first method tackles the gravity wave issue through a semi-implicit formulation studied by Robert[8] for global spectral methods; see also the work of Hack et al.[9] for a discussion. Here, the stiff (linear) terms that limit the time step through the fastest gravity wave speeds are treated with an implicit time stepping approach that effectively slows down or damps these wave modes, depending on the type of implicit time integration. While the semi-implicit approach allows significantly larger time steps, it also introduces errors that significantly increase with the time step size. The second method addresses the CFL constraint and is based on a Lagrangian formulation of the equations. This formulation overcomes the Eulerian CFL time step restrictions through the advection of Lagrangian fluid parcels along flow trajectories, resulting in larger time steps.[10] Combinations of both the abovementioned methods are frequently used in atmospheric simulations.[11,12] Like semi-implicit methods, Lagrangian methods induce errors that grow with the time step size, and avoiding such errors is obviously very desirable.

Exponential integrators are known to avoid the time step restriction for linear operators entirely, and they can be computed in various ways.[13] However, it turns out to be challenging to find a computationally efficient formulation including the Coriolis effect, which allows large time steps. An application of exponential integrators in the context of atmospheric simulations can be found, for example, in the work of Garcia et al.[14] Here, significant improvements in accuracy were observed; however, performance issues under realistic test conditions were found to be a severe issue.

PinT methods gained increasing interest over the last 50 years, and we like to refer to the work of Gander[2] for an overview. The new T-REXI time stepping method[3] studied here can be interpreted as both an exponential integrator for oscillatory systems and as a PinT algorithm that exploits additional degrees of parallelism. T-REXI approximates the oscillatory function $\exp(ix)$ by a sum over rational functions $\exp(ix) \approx \sum_i \beta_i (ix + \alpha_i)^{-1}$ with $\alpha_i, \beta_i \in \mathbb{C}$. This formulation

*Constraints of the close-to-molecular scale from physics restrict further shrinking of components.

[†]Here, we would like to prefix the term REXI with "T-" to emphasize that the REXI method of T. Haut et al. is used here. Alternative REXI-like formulations can also be based, for example, on Laplace transformations.

shares its algebraic structure with semigroups[5] and Laplace transformations.[15] Since T-REXI and Laplace transformations not only share the way how they are applied as a solver but also partly share the way how the coefficients of the rational approximation are derived, we go slightly into more detail here. First of all, both methods are based on a representation of the function to be approximated (in this work, $\exp(ix)$) in a spectral basis. For the T-REXI and Laplace methods, this is based on the Fourier and Laplace transformations, respectively. To compute the α_i and β_i coefficients for the rational approximation, T-REXI directly operates in Fourier space and uses a Fourier representation of a Gaussian basis function as a proxy to approximate $\exp(ix)$ in Fourier space, followed by merging it with a rational approximation of the Gaussian basis function. In contrast, the Laplace transformation, as it was used for example in the work of Clancy et al.,[15] uses the Cauchy contour integral method. Both methods lead to a rational approximation and, hence, share their way of how time stepping for a PDE is performed.

1.2 | Contribution and overview

In this work, we apply the T-REXI method[3] to the linearized SWE on the rotating sphere (Section 2). Section 3 provides a description of the SH used in this work. This is followed by a brief introduction to T-REXI in Section 4, which is followed by the SH-based solver for each term in T-REXI in Section 5. The efficiency of the T-REXI method is evaluated in numerical as well as performance aspects in Section 6: We study T-REXI with a standard steady-state test case used for the development of dynamical cores.[16] This is followed by a test of wave propagation over a very long time scale, which focuses on gaining a deeper understanding of wave dispersion errors in physical space. The competitiveness to other time stepping methods is shown in the context of dispersion relations via a numerical eigenvalue analysis. Finally, computational performance comparisons on the Cheyenne supercomputer are made between T-REXI and other commonly used time stepping methods.

2 | SWEs

The inviscid SWEs can be described in a very general way by $\frac{\partial}{\partial t}\mathbf{U} = \mathcal{L}(\mathbf{U}) + \mathcal{N}(\mathbf{U})$, where $\mathbf{U}$ is a 3-vector containing the prognostic state variables, $\mathcal{L}(\mathbf{U})$ is the linear operator, and $\mathcal{N}(\mathbf{U})$ is the nonlinear operator. While we recognize the critical importance of the nonlinear terms in faithfully reproducing realistic atmospheric dynamics, our intent here is to extend the T-REXI work on the linear SWE on the biperiodic plane to the rotating sphere and determine if the approach can work competitively on the rotating sphere.

Special attention has to be paid to the choice of the formulation of the SWEs. We chose the vorticity–divergence formulation (see the works of Hack et al.[9] and Temperton[17]) in which the prognostic variables are given by the geopotential $\mathbf{\Phi}$, the vorticity ζ, and divergence δ as follows:

$$\begin{bmatrix} \frac{\partial \zeta}{\partial t} \\ \frac{\partial \delta}{\partial t} \\ \frac{\partial \Phi}{\partial t} \end{bmatrix} = \begin{bmatrix} -f\delta - \mathbf{V}.(\nabla f) \\ f\zeta + \mathbf{k}.(\nabla f) \times \mathbf{V} - \nabla^2 \Phi \\ -\overline{\Phi}\delta \end{bmatrix}, \tag{1}$$

with the average geopotential $\overline{\Phi}$, $\mathbf{k}$ being a vector orthogonal to the surface, and the latitudinal-varying Coriolis effect is included with the $f = 2\Omega \sin\phi$ term. The longitude–latitude coordinates are denoted with angles λ and ϕ, respectively. $\mathbf{V} = (u, v)$ stores the velocities and is used as a diagnostic variable that can be computed based on the stream function ψ and velocity potential χ via $\mathbf{V} = \mathbf{k} \times \nabla\psi + \nabla\chi$. The stream function and velocity potential can be computed by inverting the Laplace operator in the equations $\zeta = \nabla^2\psi$ and $\delta = \nabla^2\chi$.

3 | SH

Expansions in terms of the SH functions have long been used in atmospheric dynamics solvers, particularly to invert, algebraically, similar Helmholtz operators in the context of the semi-implicit methods (e.g., CAM3,[18] ECMWF[12,19]). This past success, along with the prospect of an exact inversion of each term of the rational approximation of the exponential integrator, motivated our choice of SH for this formulation. We give a very brief introduction to SH here and to form the basis of a comprehensive description of the development of the T-REXI time stepping solver in Section 5.

The transformation of a function $\xi(\lambda, \mu)$ from *spectral* to *physical space* with the Gaussian latitude $\mu = \sin(\phi)$ is given by the approximate series expansion

$$\xi(\lambda, \mu) = \sum_{r=-R}^{R} \sum_{s=|r|}^{S(r)} \xi_s^r P_s^r(\mu) e^{ir\lambda},$$

with ξ_s^r being the spectral coefficient of the sth longitudinal mode and rth latitudinal mode. In practice with a T-truncated SH, we use a triangular truncation ($S(r) = R = T - 1$) and $s \geq r$, although more general truncations are possible. Data from *physical space* can be transformed to *spectral space* with

$$\xi_s^r = \int_{-1}^{+1} \frac{1}{2\pi} \int_0^{2\pi} \xi(\lambda, \mu) e^{-ir\lambda} d\lambda P_s^r(\mu) d\mu.$$

The $P_s^r(\mu)$ are the associated Legendre polynomials (ALPs), and the integral over the ALPs is discretized using Gaussian quadrature and requires that the latitudes are located at the quadrature points $\mu_j = \sin \phi_j$. The effective resolution of simulations is specified by the truncation of the modes, which is abbreviated with "$T[int]$." Here, T is followed by the placeholder [int] for the highest Fourier and ALP mode. Our formulation follows that of Robert,[20] who suggested scaling velocities in the SWE with $\cos \phi$. More details on the SH can be found in the works of Hack et al.[9] and Rivier et al.[21]

The properties of the SH are frequently used in global spectral methods to solve, for example, for the Laplace operator (see the works of Schreiber et al.,[4] Hack et al.,[9] and Barros et al.[12]) and for Helmholtz problems arising as part of implicit time stepping. These problems give rise to diagonal operators in spectral space.

4 | RATIONAL APPROXIMATION OF EXPONENTIAL INTEGRATORS

We now briefly introduce the background and algorithmic structure of rational approximation of exponential integrators (T-REXI) in order to lay the groundwork for the numerical analysis in Section 6.

4.1 | ODEs

T-REXI is composed of two main building blocks. The first is a rational approximation of a Gaussian function $\psi_h(x) := (4\pi)^{-\frac{1}{2}} e^{-x^2/(4h^2)} \approx \mathrm{Re}(\sum_{l=-K}^{K} \frac{a_l}{i\frac{x}{h} + (\mu + il)})$ with the coefficients μ and $a_l \in \mathbb{C}$ provided in table 1 of the work of Haut et al.[3] and h related to the width of the Gaussian function. An important numerical property is that $K = 11$ is sufficient to keep the error of this approximation close to the level of numerical double precision accuracy.[3] The second block is a linear combination of Gaussian basis functions to approximate the spectrum of the oscillatory representation $\exp(i\lambda)$, $i\lambda$ being the eigenvalues of the underlying linear system along the imaginary axis. For example, the real part of the exponential is approximated over the spectral area $[-hM; hM]$ with

$$\mathrm{Re}(e^{ix}) \approx \sum_{m=-M}^{M} \mathrm{Re}\left(b_m \psi_h(x + mh)\right) \approx \sum_n \mathrm{Re}\left(\frac{\beta_n^{\mathrm{Re}}}{ix + \alpha_n}\right), \tag{2}$$

where Re is the real part of a complex number. Here, $\beta_n^{\mathrm{Re}}, \alpha_n \in \mathbb{C}$ are complex values computed only once on initialization and M specifies the number of Gaussian basis functions used in the approximation. The approximation for the real parts of the exponential is merged with the one for the imaginary values, yielding the coefficients α_n and β_n. Finally, the sum of the rational approximation of the Gaussian function is merged with the sum for approximating the oscillations.

4.2 | PDEs

The utility of the rational approximation becomes clear when it is applied to a linear operator. Given a linear PDE $\frac{\partial}{\partial t}\mathbf{U} = L\mathbf{U}$, where L is the discretized linear operator and $\mathbf{U}$, from now on, is the discretized current state of the simulation, we can compute solutions of the simulation at time t_{n+1} with the exponential integrator formulation[13] $\mathbf{U}_{n+1} = Q \exp(\Delta t \Lambda) Q^{-1} \mathbf{U}_n$, where Λ is a matrix with (imaginary) eigenvalues on the diagonal, Q is the matrix of eigenvectors, and $\exp(\Delta t \Lambda) = \mathrm{diag}(e^{\lambda_1 \Delta t}, e^{\lambda_2 \Delta t}, \ldots, e^{\lambda_n \Delta t})$. Approximating $\exp(\Delta t \Lambda)$ with T-REXI yields $\mathbf{U}_{n+1} \approx Q \sum_{k=1}^{N} (\beta_k (\Delta t \Lambda + I\alpha_k)^{-1}) Q^{-1} \mathbf{U}_n = \sum_{k=1}^{N} \beta_k (L + I\alpha_k)^{-1} \mathbf{U}_n$. Each of these terms is independent from each other and can be solved in parallel.[3,4] We like to emphasize that REXI-based methods never require computing Q and Λ explicitly and that we use this only as an

intermediate step. It only requires solving for the complex-valued problem given by $(L + I\alpha_k)^{-1}$. Additionally, we assume that valid eigenvectors and values exist with singular eigenvalues set to zero.

4.3 | REXI with SWEs

In this section, we will develop the T-REXI formulation of the linear SWEs on the rotating sphere and will derive an efficient solver using an SH representation. For the sake of clarity, in what follows, we scale the time step size Δt to unity. We also use studies for a T-REXI formulation of the SWE on the sphere with a simplified system that assumes an unphysical constant Coriolis force. This modification of the SWE is sometimes called the f-sphere and is used for numerical studies (see, e.g., the work of Thuburn et al.[22]). We use this f-sphere approximation only for the numerical eigenvalue analysis in Section 6.3 because the eigenvalues can be computed explicitly for the f-sphere. In contrast to the f-sphere, the SWE on the rotating sphere includes the true latitudinal varying Coriolis term, and a similar approach for implicit time stepping methods was also independently developed in the work of Yessad.[23]

For T-REXI on the rotating sphere, we start with the linear operator given in advective formulation

$$\begin{bmatrix} \alpha & -\overline{\Phi}\nabla^{\lambda}. & -\overline{\Phi}\nabla^{\phi}. \\ -\nabla^{\lambda} & \alpha & f(\phi) \\ -\nabla^{\phi} & -f(\phi) & \alpha \end{bmatrix} \mathbf{U} = \mathbf{U}^0 \tag{3}$$

with $\mathbf{U}^0$ being the initial condition, $\mathbf{U} = (\Phi, u, v)^T$ being the state vector with the geopotential $\Phi = gh$, the gravity value g, height of the SWE h, and both velocity components u and v. The average geopotential is given by $\overline{\Phi} = g\overline{h}$ and α, one of the poles in the REXI sum. The superscripts λ and ϕ denote the parts of the gradient and divergence operators along the longitude or latitude, respectively. For sake of readability, we write $f = f(\phi)$. We can find an explicit formulation of the geopotential with

$$\left((\alpha^2 + f^2) - \overline{\Phi}\nabla^2\right)\Phi + \frac{\overline{\Phi}}{\alpha}F = \overline{\Phi}\left(\delta^0 - \frac{f}{\alpha}\zeta^0\right) + \left(\alpha + \frac{f^2}{\alpha}\right)\Phi^0 \tag{4}$$

and $F = f(f_\phi v + f_\lambda u) + \alpha(f_\lambda v - f_\phi u)$, where the subscripts denote the gradient along the longitude (λ) or latitude (ϕ). Unfortunately, using this equation directly does not result in an efficient solver in spectral space because the dependencies on u and v significantly increase the bandwidth and size of the matrix to solve for. However, a formulation that only depends on the geopotential can be derived as

$$\left((\alpha^2 + f^2) + \frac{\overline{\Phi}}{\alpha}F_k\nabla - \overline{\Phi}\nabla^2\right)\Phi = \overline{\Phi}\left(\delta^0 - \frac{f}{\alpha}\zeta^0\right) + \left(\alpha + \frac{f^2}{\alpha}\right)\Phi^0 - \frac{\overline{\Phi}}{\alpha}F_k\mathbf{V}^0 \tag{5}$$

with $\mathbf{V}^0 = (u^0, v^0)^T$ and $F_k = \frac{1}{\alpha^2+f^2}\nabla^{\phi} f\,[\,-(\alpha^2 - f^2), \quad 2\alpha f\,]$, where ∇^{ϕ} denotes the gradient component along the latitude. Once the geopotential Φ at the new time step is computed, we can obtain the velocities based on Equation (3) as follows:

$$\mathbf{V} = A^{-1}(\mathbf{V}^0 + \nabla\Phi) \tag{6}$$

with $A^{-1} = \frac{1}{\alpha^2+f^2}\begin{pmatrix} \alpha & -f \\ f & \alpha \end{pmatrix}$. This reformulation leads to a significant simplification of the original problem given in Equation (3), which coupled all variables given by the geopotential Φ and velocities $\mathbf{V}$. In Equation (5), the predicted geopotential Φ depends only on the initial conditions, avoiding a coupling to the velocities.

5 | REXI FOR SWEs WITH SH

In this section, we turn our attention to using the SH to find an efficient solver for Equation (5).

Our main goal is to transform Equation (5) to a form in SH spectral space $\mathcal{B}\tilde{\Phi} = \tilde{r}$, where $\mathcal{B}$ is the matrix to be inverted in spectral space, and the vector $\tilde{r}$ and $\tilde{\Phi}$ are spectral coefficients of the right-hand side and geopotential, respectively. SH recurrence identities and orthonormality properties are used to compute the matrix elements of $\mathcal{B}$. Unfortunately,

Equation (5) has the troublesome quantity $(\alpha^2 + f^2)^{-1}$ in the F_k term, which is not amenable to evaluation using ALP identities. Therefore, we multiply Equation (5) through $(\alpha^2 + f^2)$, which gives

$$\left((\alpha^2+f^2)^2 + \frac{\overline{\Phi}}{\alpha}\nabla^\phi f\left[-(\alpha^2-f^2),\quad 2\alpha f\right]\nabla - (\alpha^2+f^2)\overline{\Phi}\nabla^2\right)\Phi = (\alpha^2+f^2)\left(\overline{\Phi}\left(\delta^0 - \frac{f}{\alpha}\zeta^0\right) + \left(\alpha + \frac{f^2}{\alpha}\right)\Phi^0 + \frac{\overline{\Phi}}{\alpha}F_k\mathbf{V}^0\right). \tag{7}$$

The right-hand side $\tilde{r}$ can be directly evaluated and is partly assembled in physical space for the velocity-related components to avoid velocity-induced pole singularities in spectral space. We split the left-hand side into smaller subproblems denoted by Z_n as

$$\begin{aligned}&(\alpha^2+f^2)^2\,\Phi + \frac{\overline{\Phi}}{\alpha}\nabla^\phi f\left[-(\alpha^2-f^2),\quad 2\alpha f\right]\nabla\Phi - (\alpha^2+f^2)\overline{\Phi}\nabla^2\Phi\\ &= \alpha^4 Z_1 + 2(2\Omega)^2\alpha^2 Z_2 + (2\Omega)^4 Z_3 - \overline{\Phi}\alpha(2\Omega)Z_4 + \frac{\overline{\Phi}}{\alpha}(2\Omega)^3 Z_5 + \overline{\Phi}2(2\Omega)^2 Z_6 - \overline{\Phi}\alpha^2 Z_7 - \overline{\Phi}(2\Omega)^2 Z_8\end{aligned}$$

and find the coefficients that represent each of the Z_i functions. These functions can be derived by recurrence identities of SH. We finally assemble our matrix $\mathcal{B}$ by collecting all coefficients associated with the same SH mode of the geopotential. Once $\tilde{\Phi}$ has been calculated by solving for $\mathcal{B}$, the final step in the T-REXI solver is to compute the velocities or vorticity/divergence using Equation (6) for each term (i.e., each value of α) in the T-REXI series. The vorticity and divergence ζ^0, δ^0 are first converted to its velocity components u^0, v^0, and the entire right-hand side is evaluated. Then, the vorticity and divergence ζ, δ are computed based on the new velocity components. The T-REXI time stepping scheme for one single time step is summarized in Algorithm 1.

We close this section with a discussion on properties of the matrix $\mathcal{B}$ for which a sketch is given in Figure 1. This matrix has a low bandwidth $b = 5$ and can be solved using a backward/forward Gaussian elimination matrix inversion technique. We also note that the matrix $\mathcal{B}$ is meridionally blocked because of the pure latitude dependence of the Coriolis term. Hence, each mth zonal mode generates a system of equations that can be independently treated. This naturally exposes an additional degree of parallelization over all m modes.

Algorithm 1. Pseudo code for one single T-REXI time step by using the developed SH–REXI solver for vorticity/divergence formulation

```
Functions used in SH-REXI solver:
  S(...): Solvers for geopotential Φ and velocities (u, v)
  uv2vortdiv(...): Convert velocities to vorticity/divergence
  vortdiv2uv(...): Convert vorticity/divergence to velocities

R ∈ (ℂ^2)^N                                   ▷ REXI coefficients for N T-REXI terms

procedure SH-REXI::SOLVE(Φ̃_0, ζ̃_0, δ̃_0)      ▷ Initial conditions
    (Φ̃_new, ζ̃_new, δ̃_new) ← (0⃗, 0⃗, 0⃗)
    for all (α, β) ∈ R do                      ▷ Parallel for
        Φ̃_new ← S^Φ(Φ̃_0, ζ̃_0, δ̃_0, α)          ▷ Solve for new geopotential
        (u_0, v_0) ← vortdiv2uv(ζ̃_0, δ̃_0)      ▷ Convert vort/div to velocities
        u_tmp ← S^u(Φ̃_new, Φ̃_0, u_0, v_0, α)    ▷ Solve for u velocity
        v_tmp ← S^v(Φ̃_new, Φ̃_0, u_0, v_0, α)    ▷ Solve for v velocity
        (ζ̃_new, δ̃_new) ← uv2vortdiv(u_tmp, v_tmp)   ▷ Convert velocities to vort/div
        (Φ_new, ζ_new, δ_new) ← (Φ_new, ζ_new, δ_new) + Re((Φ_new, ζ_new, δ_new)β)   ▷ Parallel reduce operation
    end for
    return (Φ̃_new, ζ̃_new, δ̃_new)              ▷ Value of new time step
end procedure
```

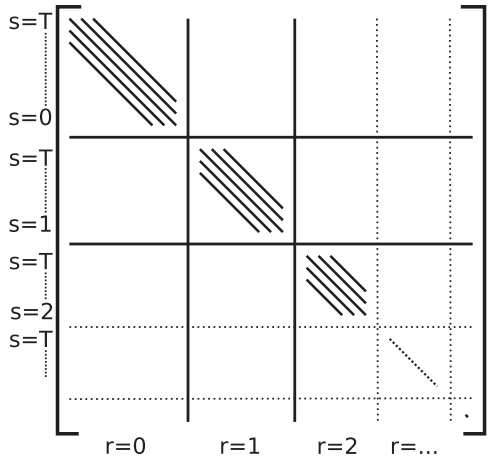

FIGURE 1 Sketch of the matrix structure to solve for the geopotential on the rotating sphere as part of the T-REXI time stepping method. There are four off-diagonals with distances ±2 and ±4 to the diagonal. The matrix is blocked for each m mode. Therefore, the linear system of equations in each partition can be solved independently to the others. T denotes the truncation for the SH (see Section 3)

6 | NUMERICAL TESTS AND PERFORMANCE RESULTS

We have conducted numerical studies to obtain a deeper understanding of T-REXI's numerical performance integrating the SWE on the rotating sphere. If not otherwise stated, we used earth parameter values $r = 6.37122 \cdot 10^6$ m, $\Omega = 7.292 \cdot 10^{-5}$ s^{-1}, $g = 9.80616$ m/s^2, and an average height of $\overline{H} = 10,000$ m. Regarding T-REXI parameters (see Section 4.1 and 4.2), the number of Gaussian basis functions for each approximation of the real and imaginary parts of the exponential function is denoted as M. In addition, the studies conducted here use a value of $h = 0.15$ for the width scaling parameter of the Gaussian basis functions. For sake of reproducability, the source code is made available in the work of Schreiber et al.[24‡]. We use SHTNS[25] library for SH transformations. For the explicit Runge–Kutta 2 method, we use the coefficients $A = (0.5)$, $b = (0, 1.0)$, and $c = (0.5)$ given in Butcher-tableau notation.

6.1 | Geostrophic balance

We first investigate the T-REXI time stepping method with a test of the stationary modes generated by a geostrophic balance between the velocity and the Coriolis effect. Considered to be a crucial test of any dynamical core,[26,27] it is also "test case 2" of a standard suite of tests[16] for the SWE, and we use a linearized version of this originally nonlinear benchmark. We generate the geostrophic balance with the following initial conditions: a zero meridional velocity $v = 0$, a zonal velocity $u(\lambda, \phi) = u_0 \cos\phi$ with $u_0 = 2\pi r/12$, and the geopotential given by $\Phi(\lambda, \phi) = g\overline{H} + u_0 r\Omega\cos^2\phi$. The time derivatives generated by the geopotential balance with the Coriolis term are zero. This benchmark is in particular interesting for studying T-REXI because it is not explicitly formulated in terms of time derivatives in contrast to, for example, explicit Runge–Kutta methods that solely rely on time derivatives and with the time derivatives being analytically zero for this particular benchmark. We conducted studies over a simulation time of 1 on the unit sphere and set $g = \overline{H} = f = 1$ as well, which allows us to discriminate between round-off and time stepping errors. We used a time step size of $\Delta t_{\text{RK2}} = 0.01$ for RK2 methods and a 10 times larger time step size of $\Delta t_{\text{T-REXI}} = 0.1$ for T-REXI. All studies are conducted on an effective resolution of $T64$ (see Section 3).

The time-dependent errors in the height field in the ℓ_∞ norm are given in Figure 2. The T-REXI experiments were conducted with varying numbers of Gaussian basis functions $M = \{2^n | 0 \leq n \leq 8\}$. The RK2 time stepping method shows the expected very high double precision accuracy of $O(10^{-13})$, and we like to mention here that this small error is only possible because the steady-state test case is designed to provide zero time derivatives. RK2 is solely based on time derivatives; hence, errors directly cancel out and significant errors with RK are visible in other benchmarks in the next sections. T-REXI, which is not based on the time derivatives, displays errors that are considerably higher, even for relatively large numbers of T-REXI terms. The source of this is a T-REXI error that was traced to a subtle issue in the coefficients used in a rational approximation $e^{ix} \approx \sum_n \beta_n (\alpha_n + ix)^{-1}$. Tests for $x = 0$ (related to stationary modes that are

‡Repository,[24] commit from 2018-06-04, benchmarks in `benchmarks_sphere/sph_rexi_linear_paper_*`

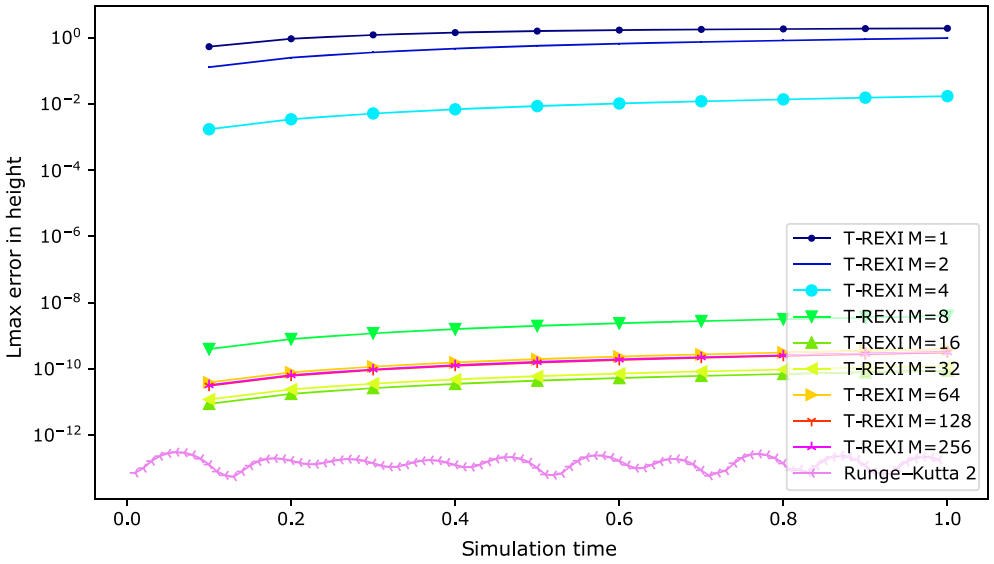

FIGURE 2 Geostrophic balance benchmark for the rational approximation of exponential integrators (T-REXI) coefficients, which were *not optimized for geostrophic balance*: The plot shows the maximum error of height field versus simulation time. High accuracy for the RK2 method is apparent; however, the T-REXI time stepping method errors are consistently much larger, even after a single time step

the only ones in this benchmark) with $M = 128$ T-REXI poles reveal a residual error of

$$1 - e^{i0} \approx \sum_n \beta_n (\alpha_n + i0)^{-1} = 1 - \sum_n \frac{\beta_n}{\alpha_n} = -1.559352647 \cdot 10^{-11} = \epsilon. \tag{8}$$

This small error can become a concrete issue when trying to obtain geostrophic balance for T-REXI using the SH method. Our ad hoc solution was to rescale the β_n coefficients with this residual ϵ^{-1}. Strongly improved results are obtained using the renormalized β_n coefficients, with T-REXI errors of $O(10^{-12})$, as are shown in shown Figure 3. We close this section with a brief discussion of T-REXI error growth in the geostrophic balance case. Let $1 - \epsilon$ be the REXI response to the geostrophic modes at $x = 0$, which is expected to be 1 and $\epsilon > 0$. After N time steps, the maximum response error to the geostrophic modes is $(1 - \epsilon)^N$ and the T-REXI error growth can be estimated as $\epsilon_T = (1 - \epsilon)^N - 1$. The number

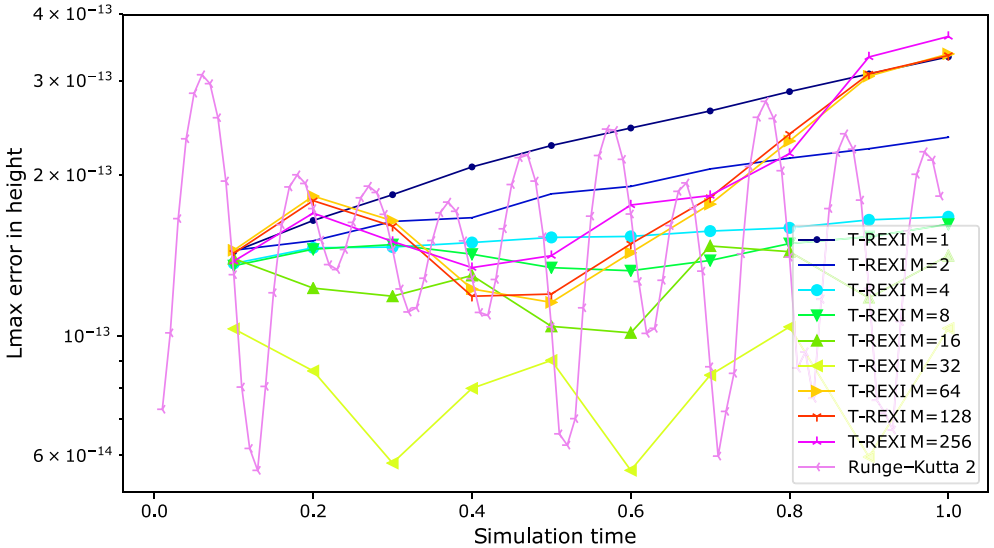

FIGURE 3 Geostrophic balance benchmark for different rational approximation of exponential integrators (T-REXI) coefficients M. The T-REXI poles are *optimized for geostrophic balance* by renormalizing the rational approximation for accurate representation of zero eigenvalues. The ℓ_∞ error of the height field versus the simulation time is shown. The values at the simulation time 0 are omitted. The T-REXI time stepping results are significantly improved up to the order of double precision accuracy

of T-REXI time steps leading to an error of ϵ_T is then given by $N = \log_{1+\epsilon} |1 - \epsilon_T|$. Thus, a cumulative error $\epsilon_T = 10^{-6}$ equivalent to single precision would therefore be introduced after about 60,000 T-REXI time steps, an issue only relevant for simulations that demand highly accurate time integration of stationary modes.

6.2 | Propagation of Gaussian bumps

In this section, we compare wave propagation in T-REXI to the nth order Runge–Kutta (RKn) and Crank–Nicolson (CN) time stepping methods. The test case that we have created is designed to help analyze and visualize dispersion errors in numerical methods. The initial state begins at rest ($u = v = 0$) with a displacement of the surface height with a Gaussian-shaped function or "bump" of the form

$$d(\lambda_1, \phi_1, \lambda_2, \phi_2) = \operatorname{acos}(\sin\phi_1 \sin\phi_2 + \cos\phi_1 \cos\phi_2 \cos(\lambda_1 - \lambda_2))$$
$$\psi(\lambda, \phi, \lambda_c, \phi_c, p) = \exp\left(-d(\lambda_c, \phi_c, \lambda, \phi)^2 \cdot p\right) 0.1\overline{H},$$

with the superscript c denoting the coordinates of the Gaussian bump and p controls its width. To cover a larger area of the power spectrum, we use a superposition of three Gaussian bumps of different widths as follows:

$$H(\lambda, \phi) = \overline{H} + \psi\left(\lambda, \phi, 0.2\pi, \frac{1}{3}\pi, 20\right) + \psi\left(\lambda, \phi, 1.2\pi, -\frac{1}{5}\pi, 80\right) + \psi\left(\lambda, \phi, 1.6\pi, -\frac{1}{4}\pi, 360\right).$$

The simulation is executed for 1.5 days using earth-like physical parameters, and a $T128$ SH truncation scheme was used (see Section 3). During the test, the Gaussian bumps propagate over the sphere as disturbances and, finally, reassembles

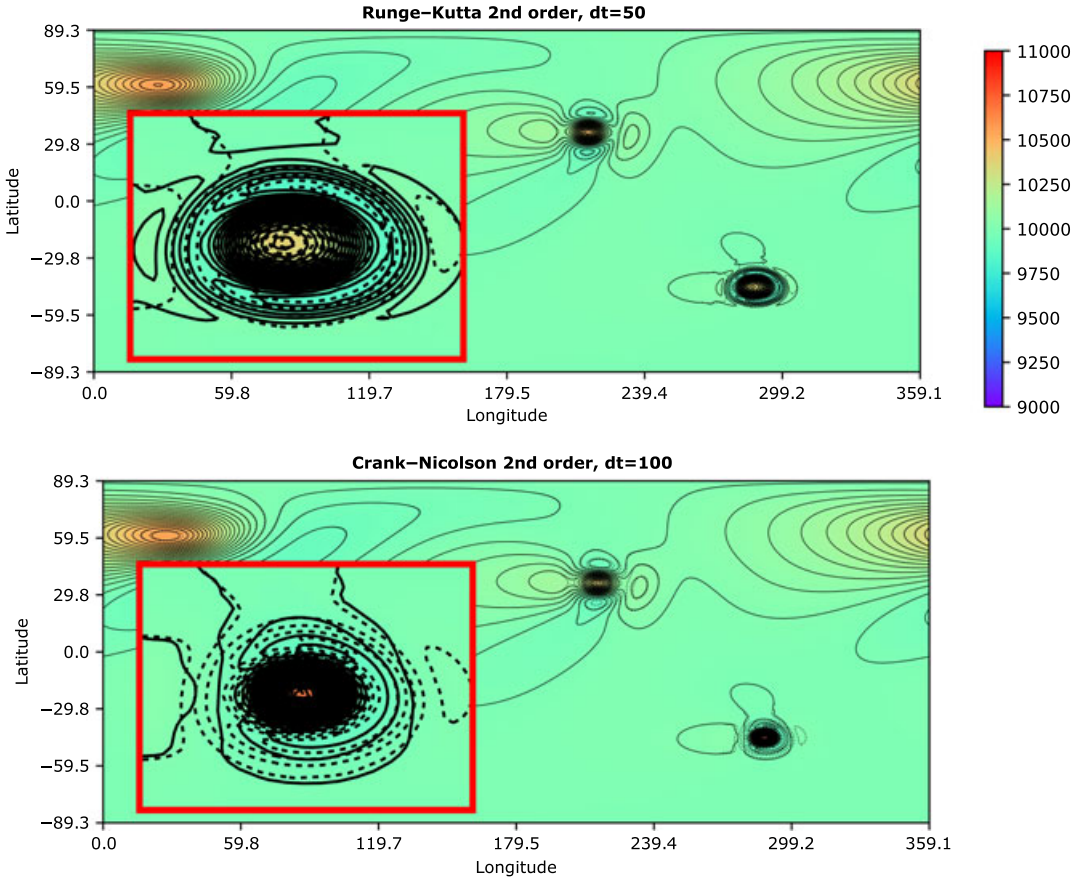

FIGURE 4 Comparison of the surface height field produced for two different time stepping methods after 1.5 days. The three Gaussian bumps have closely reassembled themselves. The reference solution (dashed lines) is compared to the results of each method (solid isolines). The red rectangle zooms in on one of the bumps closest to the south pole. Results with $\Delta t = 50$ s closely resemble the reference solution (only second-order Runge–Kutta [RK2] is shown here). For the Crank–Nicolson (CN) method with a 100 s time step, dispersion errors (expressed by nonmatching isolines) are clearly visible. Further increases of the time step size led to instabilities for the RK2 method and even worse mismatches of the isolines for CN

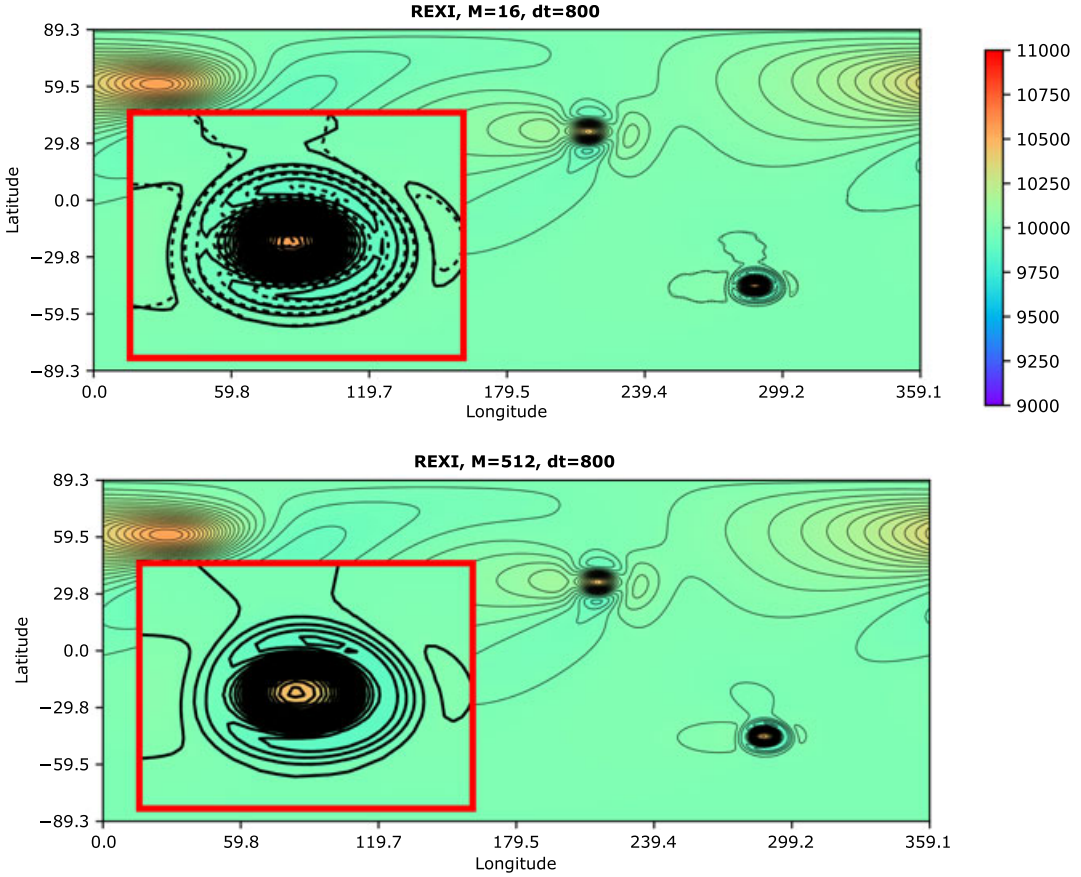

FIGURE 5 The surface height field produced after 1.5 simulated days using the T-REXI time integration scheme is compared to the RK4 reference solution, again printed with dashed isolines. A time step of 800 s was used for T-REXI. The first plot shows considerable errors in the propagation due to an insufficient number of T-REXI poles (M = 16 in this case). The second plot shows very accurate results for T-REXI with $M = 512$, compared with RK2 and CN results from Figure 4

themselves near their original positions. For all studies, we generate a reference height (H) solution using an explicit RK4 method and a time step size of 50 s. In the following results, the reference solution is plotted as dashed isolines at intervals of $\Delta H = 30$ m relative to the average height $\overline{H}$.

In Figure 4, the dispersion errors for commonly used second-order time stepping methods are compared with the fourth-order (RK4) reference solution. For a time step size of $\Delta t = 50$ s, all second-order in time methods give reasonable solutions, although errors can be observed even for this relatively small time step size (only the RK2 results (top panel) are shown). Doubling the time step to $\Delta t = 100$ s leads to visible instabilities[§] for RK2, and CN methods show significantly increased dispersion errors visible as nonmatching isolines in the lower panel.

We now turn to comparisons of the T-REXI method with the RK4 reference solution. Figure 5 shows T-REXI solutions $\Delta t = 800$ s, already 16 times larger than RK2. The T-REXI solution in the upper panel ($M = 16$) shows significant errors. This is due to using a small number of poles, insufficient to approximate the eigenvalue spectrum. However, increasing the number of T-REXI integration poles to $M = 512$ leads to a highly accurate solution (lower panel).

In Figure 6, we compare T-REXI with the RK4 reference solution when T-REXI takes one enormous 1.5 day time step. For the T-REXI $M = 1{,}024$ case, significant errors are again generated (top panel). However, increasing the number of T-REXI integration poles to $M = 4{,}098$ again restores agreement with the reference solution. Perhaps remarkably, T-REXI is able to yield a higher accuracy solution than the RK2 method (top panel of Figure 4), using a 2,592 times larger time step.

[§]We would like to mention here that RK2 has known problems for oscillatory problems, however provided stable results within the chosen time integration interval.

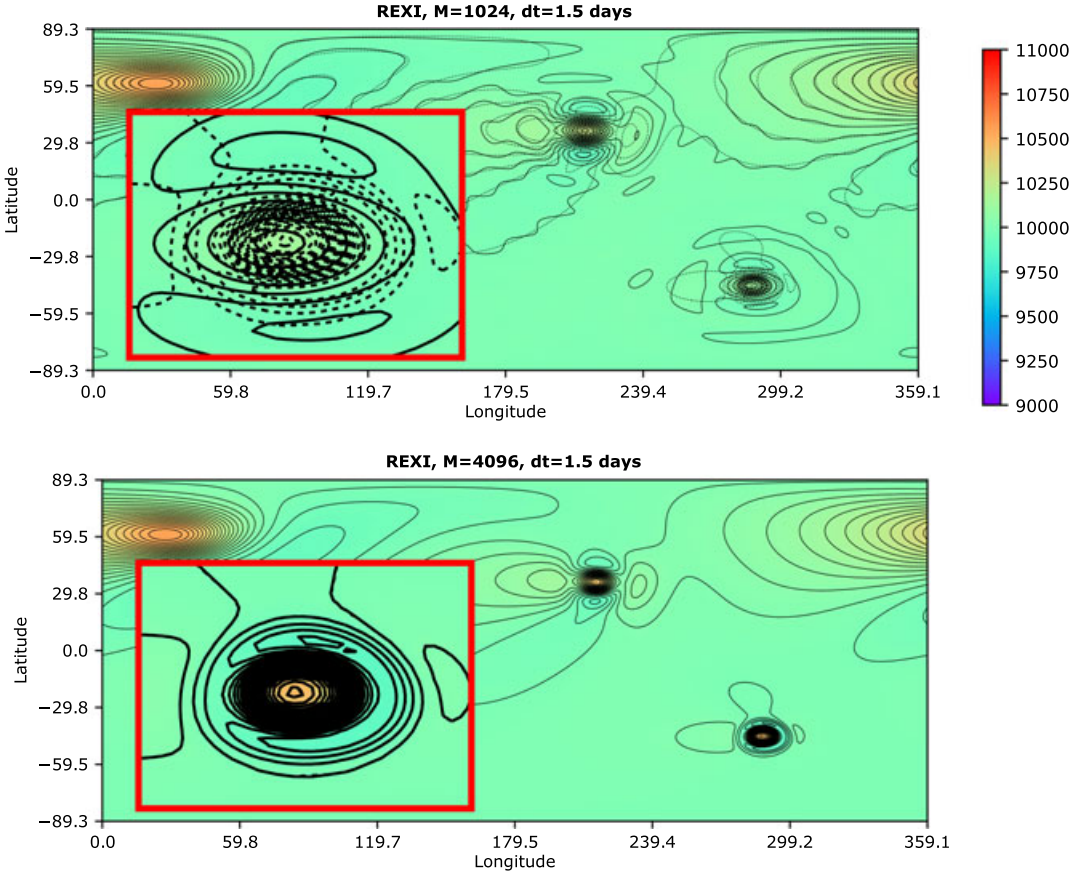

FIGURE 6 This figure is the same as Figure 5 but with T-REXI time step set to 1.5 days. The RK4 reference solution is computed and plotted as before. The first plot (upper panel) shows significant errors in the solution with the T-REXI $M = 1024$: Accuracy is restored in the lower panel using $M = 4{,}192$. The results obtained are of higher accuracy than the solution computed with the RK2 method

6.3 | Numerical dispersion analysis

In this section, we provide an in-depth numerical analysis of the dispersion relations of T-REXI versus other time stepping methods. Explicit and implicit methods are known to suffer from either accelerating or decelerating the dispersion speeds of waves (see the works of Hoskins et al.,[28] Durran,[29] and Lynch[30]). In this section, we use a mode analysis to reveal dispersion properties and errors; see, for example, the works of Thuburn et al.,[22] Weller et al.,[31] and Peixoto.[32] Dispersion errors due to spatial discretization are avoided by our choice of the global SH method, which allows us to cleanly isolate the dispersion errors arising from the time stepping methods alone. Due to computational complexity of an eigenvalue decomposition, this study used a reduced T16 wave number truncation scheme (see Section 3).

We analyze the dispersion relations over a sufficiently large time such that dispersion errors in the time stepping method itself are revealed. Given the matrix E that integrates $\mathbf{U}_n$ to $\mathbf{U}_{n+1}$, we obtain the dispersion relations in Λ by using an eigenvector/value formulation for exponential integrators with $\mathbf{U}_{n+1} = E\mathbf{U}_n = Qe^{\Delta t\Lambda}Q^{-1}\mathbf{U}_n$. Taking the logarithm of the eigenvalues of E then reveals details on the dispersion modes. Special attention is required since the logarithm on complex numbers is not bijective: The eigenvalues obtained might not be related to the real ones but might be to ones shifted by multiples of 2π, yet still yielding the correct results. We used a maximum time integration interval of $\Delta t = 400$ s, which assures a bijective property. The linear operator matrix E itself is obtained by iterating over all modes of the state vector $\mathbf{U}_n$. In each iteration, only the current mode is activated and a time step is executed. The resulting state vector $\mathbf{U}_{n+1}$ then represents one column of the linear operator matrix E.

We performed studies on the f-sphere with the results provided in Figure 7. In general, there are significant errors for first- and second-order accurate methods. The RK2 method accelerates waves, whereas all other considered methods decelerate them (see also the work of Durran[29]). The fourth-order accurate Runge–Kutta method results in relatively small errors that are significantly smaller than those for second-order accurate methods.

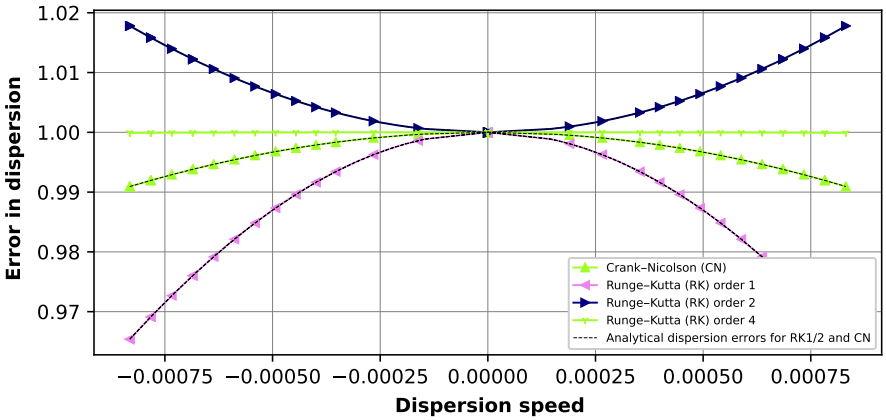

FIGURE 7 Relative phase errors for Runge–Kutta of order 1, 2, and 4 and Crank–Nicolson based on the linear shallow-water equation computed with spherical harmonics. We can observe significant errors for second-order accurate time stepping methods for fast-moving waves (see also the work of Durran[29]). Markers are set for every 10th mode

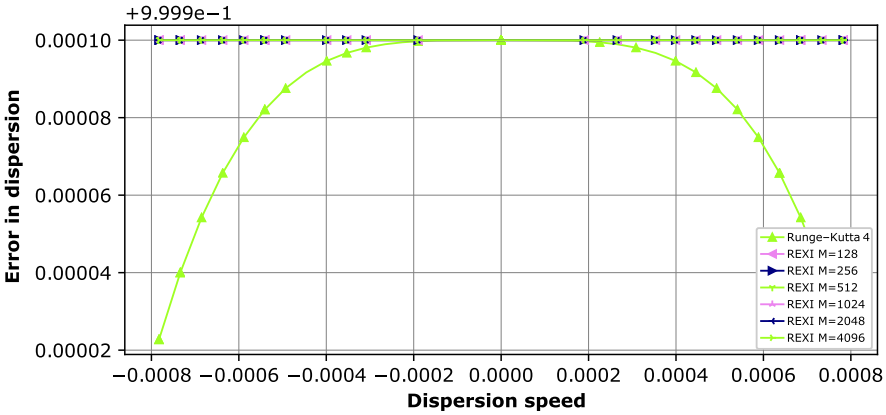

FIGURE 8 Relative phase errors for T-REXI and RK4 with the linear shallow-water equation computed with spherical harmonics. We can observe that T-REXI is able to cope significantly better with fast waves. Markers are set for every 10th mode. REXI, rational approximation of exponential integrators

To show the potential of T-REXI, we compare it to RK4 in Figure 8. Here, RK4 still results in larger errors for fast-moving waves. In contrast, T-REXI does not show increased wave dispersion errors for faster moving waves in the given example.

6.4 | Performance comparison with massively parallel REXI

Next, we compare the computational performance of T-REXI with conventional time stepping methods. All performance results are conducted on the Cheyenne supercomputer.[33] The performance metric we adopt for our performance intercomparison is based on the wall clock time required to perform a full time integration of 1.5 days. The benchmark setup is identical to the propagating Gaussian bumps from Section 6.2. The reference solution was computed with a Runge–Kutta 4 method and $\Delta t = 50$ s, and the errors are computed with the ℓ_∞ norm to the reference height. We used RK2 and CN as conventional time stepping methods and executed them using only a single core on an exclusively reserved nonuniform memory access domain. Using more cores would be only beneficial for a significantly increased workload (e.g., by significantly increasing the resolution or extending it to the vertical). For RK2, time step sizes $\Delta t \geq 100$ s turned out to be unstable, and despite being stable, for CN, time step sizes of $\Delta t \geq 150$ s resulted in significant errors (see Section 6.2). For T-REXI, we conducted different studies ($\Delta t = \{800\text{ s}, 1600\text{ s}, 1.5\text{ days}\}$, $M = \{512, 1024, 4096\}$) and distributed the PDEs of each REXI term equally across $N = \{2^i | i \leq 0 < 10\}$ compute ranks. We use only one rank per socket (two per compute node) to maximize the available bandwidth to solve for each term in the T-REXI formulation. Hence, the maximum number of used compute nodes on Cheyenne is $\frac{2^9 \text{ MPI ranks on one socket}}{2 \text{ sockets per node}} = 256$.

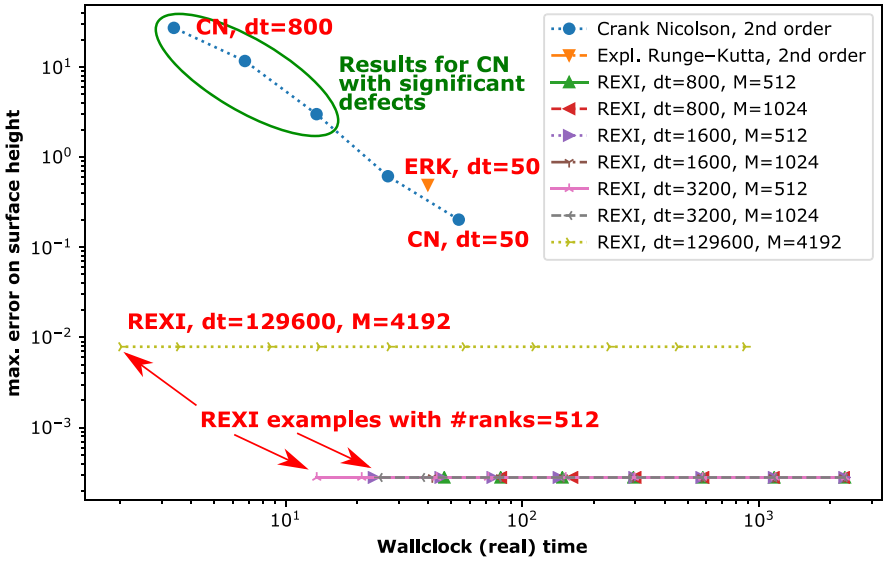

FIGURE 9 Wall clock versus error on the difference in surface height comparing explicit Runge–Kutta (ERK), Crank–Nicolson (CN), and rational approximation of exponential integrators (T-REXI) time stepping methods. We can observe that runs based on T-REXI always result in improved accuracy compared to the other time stepping methods. Based on the results in a previous section, it is important to mention that CN time stepping results with $\Delta t > 100$ s are of no use due to significant errors. T-REXI time stepping uses up to 512 additional compute ranks and shows significant improvements regarding the time to error compared with other time stepping methods

The results are given in Figure 9. Using T-REXI always results in errors that are lower than for the conventional time stepping methods. Therefore, for the studied conventional methods, only a further reduction of time step size would make them competitive, however also increasing their wall clock time. Given the best wall clock time of 27.1 s for the conventional TS method CN with $\Delta t = 100$ s and comparing it to the best REXI method with $M = 512$ and $\Delta t = 3,200$ s with a wall clock time of 13.5 s reveals a speedup of 2.0×. Even if we do not expect that time step sizes of 1.5 days with a wall clock time of 2.02 s can be used once including the nonlinearities, we would like to mention the potential wall clock speedup of 13.4× if a way to incorporate the nonlinearities can be found as part of future research. We also like to mention that the scalability limitation with $M = 4,096$ T-REXI terms was not yet reached because we only used 512 compute ranks.

7 | SUMMARY AND FUTURE WORK

The apparent advantages of Haut et al.'s[3] T-REXI method are that it allows, for linear oscillatory operators, (a) arbitrarily long time steps and (b) a realization with a sum over the solutions to a series of embarrassingly parallel solvers of the form $\mathbf{U}_{n+1} \approx \sum_i \beta_i (\alpha_i + \Delta t L)^{-1} \mathbf{U}_n$. In this work, we applied T-REXI to the linear terms of the SWEs on the rotating sphere. Applying T-REXI to all linear terms of this SWE requires coping with the Coriolis term induced by the rotating sphere and leads to additional challenges. These have been overcome through a formulation that solves for the geopotential alone, reducing the complexity of the system of equations by a factor of three. Once the geopotential is obtained, it is straightforward to directly compute the velocities. Using an SH method enables the formulation of T-REXI's $(\alpha_i + \Delta t L)^{-1}$ term for the rotating SWE as a low-bandwidth matrix in spectral space with the bandwidth independent of the resolution: This leads immediately to the required efficient direct solver. Additionally, we can avoid dispersion errors (up to numerical precision) of gravity and Rossby waves, which are both of significant importance in the atmosphere.

Three test cases relevant to atmospheric simulations were conducted for this approach: geostrophic balance, Gaussian breaking dams, and wave dispersion. The geostrophic balance stability test case revealed small SH modal errors, which a simple normalization of T-REXI coefficients resolved. We assessed T-REXI's numerical performance with a propagation of three differently sized Gaussian bumps across the earth over 1.5 simulated days and compared the dispersion errors of the T-REXI scheme to two widely used time stepping methods (Runge–Kutta 2, Crank–Nicolson). T-REXI was able to take a single 1.5 day time step that led to smaller solution errors than those achieved by the established methods requiring

much smaller time steps. The price to pay for this was to increase the number of T-REXI terms to 4,096, however exposing the potential to parallelize over these terms.

The ability of a numerical method to accurately reproduce the dispersion of waves in the SWE is of particular interest for climate and weather simulations, where tracking atmospheric effects and their interactions accurately over long time integration intervals is required. Here, wave dispersion relations for widely used time stepping methods were extracted and particular defects for fast-moving waves were observed. T-REXI avoided significant wave dispersion errors while taking larger time step sizes. All our studies demonstrated T-REXI's superior properties regarding its dispersion relations.

We conducted performance studies on the Cheyenne supercomputer by parallelizing over the T-REXI terms. Using a time step size that is 32 time larger than using a Crank–Nicolson method, the wall clock time is reduced by 2.0× and the errors are significantly reduced. Taking T-REXI to its extreme, we also performed one large 1.5-day time step with $M = 4{,}096$ using T-REXI, which resulted in a significant reduction of the errors and yielded a speedup of 13.4×, with the scalability limitation not yet reached.

In summary, our results show that T-REXI can be successfully extended to the rotating sphere, can take very large time steps in the case of the stiff linear oscillatory terms of the SWE, and is competitive to other time stepping schemes. The embarrassingly parallel set of matrix inversion problems at the heart of T-REXI is well aligned with modern computing technology trends. However, some limitations and obvious extensions of the current work are worth noting. First, methods based on SH have well recognized numerical and computational limitations that have led many in the atmospheric community to turn to other approaches. Therefore, the application of T-REXI to other numerical schemes using scalable iterative solvers should be investigated. Second, while our focus on applying T-REXI to the linear parts of the SWE on the rotating sphere is an appropriate first step, we fully expect that extensions of this work to the fully nonlinear SWE are required and would likely lead to time step restrictions on the T-REXI scheme. Such extensions to the nonlinearities can be accomplished in different ways such as Strang splitting, nonlinear exponential integrators, and other PinT methods (ParaEXP,[34] aPinT[35]). Unfortunately, the severity of these restrictions regarding wall clock time to solution, including the nonlinear interactions and how to overcome them for the SWE on the rotating sphere, is not yet researched. These challenges remain, therefore, important topics for future research in the development of (REXI-based) PinT methods.

ACKNOWLEDGEMENTS

We would like to acknowledge computation time for early computational studies on the Yellowstone cluster[36] and the MAC cluster at TUM. We would like to acknowledge high-performance computing support from Cheyenne[33] (doi:10.5065/D6RX99HX) provided by NCAR's Computational and Information Systems Laboratory, sponsored by the National Science Foundation. Martin Schreiber likes to thank Pedro S. Peixoto, Nathanaël Schaeffer, Nils Wedi, Terry Haut, Jemma Shipton, Houjun Wang, and Beth Wingate for various discussions over the last 2.5 years. We would like to thank the anonymous reviewers for their valuable feedback that strongly improved the focus of this paper on the T-REXI method.

ORCID


Martin Schreiber http://orcid.org/0000-0002-2390-6716

REFERENCES

1. Dennard RH, Gaensslen FH, Rideout VL, Bassous E, Leblanc AR. Design of ion-implanted MOSFET's with very small physical dimensions. IEEE J Solid State Circuits. 1974;9(5):256–268.
2. Gander MJ. 50 years of time parallel time integration. In: Carraro T, Geiger M, Körkel S, Rannacher R, editors. Multiple shooting and time domain decomposition. New York, NY: Springer-Verlag; 2015.
3. Haut T, Babb T, Martinsson PG, Wingate BA. A high-order time-parallel scheme for solving wave propagation problems via the direct construction of an approximate time-evolution operator. IMA J Numer Anal. 2015;36:688–716.
4. Schreiber M, Peixoto PS, Haut T, Wingate B. Beyond spatial scalability limitations with a massively parallel method for linear oscillatory problems. Int J High Perform Comput Appl. 2017.
5. Hochbruck M, Ostermann A. Exponential integrators. Acta Numerica. 2010;19:209–286.
6. Kasahara A. Numerical integration of the global barotropic primitive equations with Hough harmonic expansions. J Atmospheric Sci. 1977;34(5):687–701.
7. Wang H, Boyd JP, Akmaev RA. On computation of Hough functions. Geosci Model Dev. 2016;9(4):1477–1488.

8. Robert A. The integration of a spectral model of the atmosphere by the implicit method. In: Proceedings of the WMO/IUGG Symposium on Numerical Weather Prediction; 1969; Tokyo, Japan. Tokyo, Japan: Japan Meteorological Agency; 1969. p. 19–24.
9. Hack JJ, Jakob R. Description of a global shallow water model based on the spectral transform method. NCAR Technical Note NCAR/TN-343+STR. Boulder, CO: National Center for Atmospheric Research; 1992.
10. Ritchie H. Application of the semi-Lagrangian method to a spectral model of the shallow water equations. Mon Weather Rev. 1988;116(8):1587–1598.
11. Wood N, Staniforth A, White A, et al. An inherently mass-conserving semi-implicit semi-Lagrangian discretization of the deep-atmosphere global non-hydrostatic equations. Q J Royal Meteorol Soc. 2014;140(682):1505–1520.
12. Barros SRM, Dent D, Isaksen L, Robinson G, Mozdzynski G, Wollenweber F. The IFS model: a parallel production weather code. Parallel Computing. 1995;21(10):1621–1638. Climate and weather modeling.
13. Moler C, Van Loan C. Nineteen dubious ways to compute the exponential of a matrix, twenty-five years later. SIAM Review. 2003;45(1):3–49.
14. Garcia F, Bonaventura L, Net M, Sánchez J. Exponential versus IMEX high-order time integrators for thermal convection in rotating spherical shells. J Comput Phys. 2014;264:41–54.
15. Clancy C, Lynch P. Laplace transform integration of the shallow-water equations. Part I: Eulerian formulation and Kelvin waves. Q J Royal Meteorol Soc. 2011;137(656):792–799.
16. Williamson DL, Drake JB, Hack JJ, Jakob R, Swarztrauber PN. A standard test set for numerical approximations to the shallow water equations in spherical geometry. J Comput Phys. 1992;102(1):211–224.
17. Temperton C. On scalar and vector transform methods for global spectral models. Mon Weather Rev. 1991;119(5):1303–1307.
18. Collins WD, Rasch PJ, Boville BA, et al. Description of the NCAR community atmosphere model (CAM 3.0). NCAR Technical Note NCAR/TN-464+STR. Boulder, CO: National Center for Atmospheric Research; 2004.
19. White PW. IFS documentation: Part III: Dynamics and numerical procedures (CY21r4). Reading, UK: European Centre for Medium-Range Weather Forecasts; 2000.
20. Robert AJ. The integration of a low order spectral form of the primitive meteorological equations. J Meteorol Soc Jpn Ser II. 1966;44(5):237–245.
21. Rivier L, Loft R, Polvani LM. An efficient spectral dynamical core for distributed memory computers. Mon Weather Rev. 2002;130(5):1384–1396.
22. Thuburn J, Ringler TD, Skamarock WC, Klemp JB. Numerical representation of geostrophic modes on arbitrarily structured C-grids. J Comput Phys. 2009;228(22):8321–8335.
23. Yessad K. Semi-implicit spectral computations and predictor-corrector schemes in the cycle 43 of ARPEGE/IFS. 2016. Available from: https://www.umr-cnrm.fr/gmapdoc/IMG/pdf/yksi43.pdf
24. Schreiber M, Peixoto P, Schmitt A. SWEET software. 2017. Available from: https://github.com/schreiberx/sweet, https://schreiberx.github.io/sweetsite/
25. Schaeffer N. Efficient spherical harmonic transforms aimed at pseudospectral numerical simulations. Geochem Geophys Geosystems. 2013;14(3):751–758.
26. Staniforth A, Thuburn J. Horizontal grids for global weather and climate prediction models: a review. Q J Royal Meteorol Soc. 2012;138(662):1–26.
27. Thuburn J, Cotter CJ. A framework for mimetic discretization of the rotating shallow-water equations on arbitrary polygonal grids. SIAM J Sci Comput. 2012;34(3):B203–B225.
28. Hoskins B, Simmons AJ. A multi-layer spectral model and the semi-implicit method. Q J Royal Meteorol Soc. 1975;101(429):637–655.
29. Durran DR. Numerical methods for fluid dynamics: With applications to geophysics. Vol. 32. New York, NY: Springer Science & Business Media; 2010.
30. Lynch P. The emergence of numerical weather prediction: Richardson's dream. Cambridge, UK: Cambridge University Press; 2006.
31. Weller H, Thuburn J, Cotter CJ. Computational modes and grid imprinting on five quasi-uniform spherical C grids. Mon Weather Rev. 2012;140(8):2734–2755.
32. Peixoto PS. Accuracy analysis of mimetic finite volume operators on geodesic grids and a consistent alternative. J Comput Phys. 2016;310:127–160.
33. Computational and Information Systems Laboratory. Cheyenne: SGI ICE XA System (NCAR Community Computing). Boulder, CO: National Center for Atmospheric Research; 2017. Available from: https://doi.org/10.5065/D6RX99HX
34. Gander MJ, Guettel S. Paraexp: a parallel integrator for linear initial-value problems. SIAM J Sci Comput. 2013;35(2):C123–C142.
35. Haut TS, Wingate BA. As asymptotic parallel-in-time method for highly oscillatory PDEs. SIAM J Sci Comput. 2014;36(2):A693–A713.
36. Computational and Information Systems Laboratory. Yellowstone: IBM iDataPlex System (NCAR Community Computing). Boulder, CO: National Center for Atmospheric Research; 2012. Available from: http://n2t.net/ark:/85065/d7wd3xhc

How to cite this article: Schreiber M, Loft R. A parallel time integrator for solving the linearized shallow water equations on the rotating sphere. *Numer Linear Algebra Appl*. 2018;e2220. https://doi.org/10.1002/nla.2220